Also see separate doc file for clarification of corrections if necessary ("Lynch & Barry, corrections.doc")

9 Ligand-Gated Ion Channels: Permeation and Activation[1]

Joseph W. Lynch and Peter H. Barry

9.1 Introduction

Ligand-gated ion channels (LGICs) are fast-responding channels in which the receptor, which binds the activating molecule (the ligand), and the ion channel are part of the same nanomolecular protein complex. This chapter will describe the properties and functions of the nicotinic acetylcholine LGIC superfamily, which play a critical role in the fast chemical transmission of electrical signals between nerve cells at synapses and between nerve and muscle cells at endplates. All the processing functions of the brain and the resulting behavioral output depend on chemical transmission across such neuronal interconnections. To describe the properties of the channels of this LGIC superfamily, we will mainly use two examples of this family of channels: the excitatory nicotinic acetylcholine receptor (nAChR) and the inhibitory glycine receptor (GlyR) channels. In the chemical transmission of electrical signals, the arrival of an electrical signal at the synaptic terminal of a nerve causes the release of a chemical signal—a neurotransmitter molecule (the ligand, also referred to as the agonist). The neurotransmitter rapidly diffuses across the very narrow 20–40 nm synaptic gap between the cells and binds to the LGIC receptors in the membrane of the target (postsynaptic) cell and generates a new electrical signal in that cell (e.g., Kandel et al., 2000). How this chemical signal is converted into an electrical one depends on the fundamental properties of LGICs and the ionic composition of the postsynaptic cell and its external solution.

§1 / i.e., "Kandel"

The LGICs are small highly specialized protein complexes, about 12 nm long and 8 nm in diameter, which span the 3 nm or so lipid bilayer membranes of the nerve or muscle cells (see Fig. 9.1). Many of these fast neurotransmitter channels belong to the nicotinic acetylcholine superfamily of LGICs, which are also referred to as the Cys-loop superfamily of LGICs (because of the presence of a conserved signature Cys-loop, loop 7, which is present in all family members, as shown for the GlyR in Fig. 9.2, in Section 9.2). Although other ligand-gated ion channels exist, we will be confining ourselves to this superfamily, whose members are all closely

[1] This chapter is a revised and expanded version of Barry and Lynch (2005), and portions of that paper are reprinted, with permission, from *IEEE Trans. Nanobiosci.*, vol. 4, no. 1, pp. 70–80, Mar. 2005 IEEE.

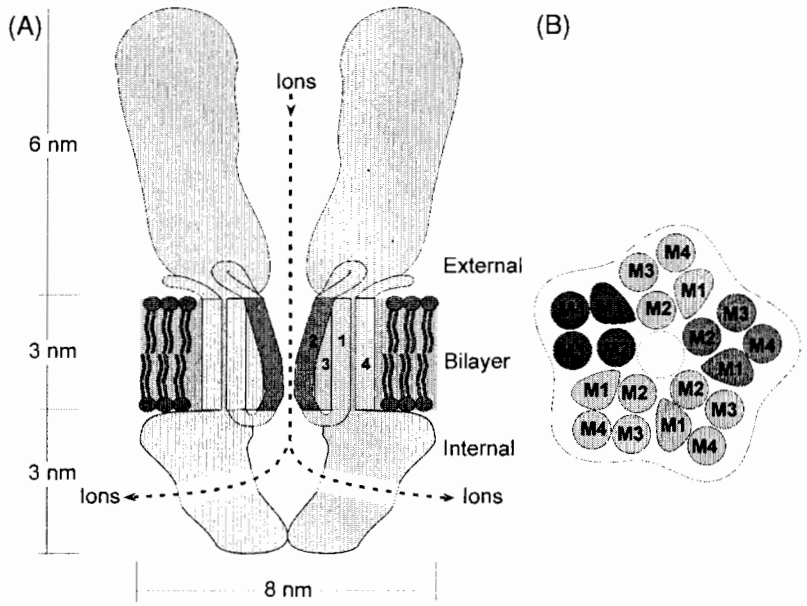

Fig. 9.1 Schematic longitudinal and cross-sectional diagrams of a typical LGIC. (Originally modified from Fig. 1 of Keramidas et al., 2004, and based on Unwin, 1993; Miyazawa et al., 1999; and Brejc et al., 2001). Panel A shows two of the five subunits and the pathway for ions entering the exterior end of the channel and moving into the cell interior via lateral portals at the cytoplasmic end of the channel, as in the nAChR channel. The numbers 1–4 refer to the M1–M4 segments for each subunit. Panel B shows a cross-sectional view of the LGIC with the four transmembrane segments of each of the five subunits. It also illustrates the five M2 segments, lining the pore region of the channel within the membrane lipid bilayer. The figure has been reproduced in monochrome from Fig. 1 of Barry and Lynch (2005), with copyright permission of [2005] IEEE.

related genetically and are very similar structurally and mechanistically, though their precise physiological function can be quite different.

When the appropriate chemical neurotransmitter, the ligand, binds to the LGIC, which incorporates both the receptor and the ion channel, the action of the ligand binding to its docking site on the receptor can somehow then cause the channel to open. The open channel selectively allows certain species of ions to pass from one side of the cell membrane to the other, through the channel. The magnitude and direction of the resulting current depends on the signs of the permeating ions and their electrochemical potential energy gradient across the membrane. The LGICs can exist in three main states. They are normally closed in the absence of the binding of any ligand, will very rapidly open within about 20 μs of the ligand binding and will close when the ligand dissociates from the receptor. However, in the continued presence of a relatively high concentration of ligand, they can also go into a third desensitized, nonconducting, state, while the ligand is still bound. This is functionally similar to the closed state except that it cannot be opened by the further addition of ligand molecules. In the desensitized state, the LGIC is unable to be reactivated

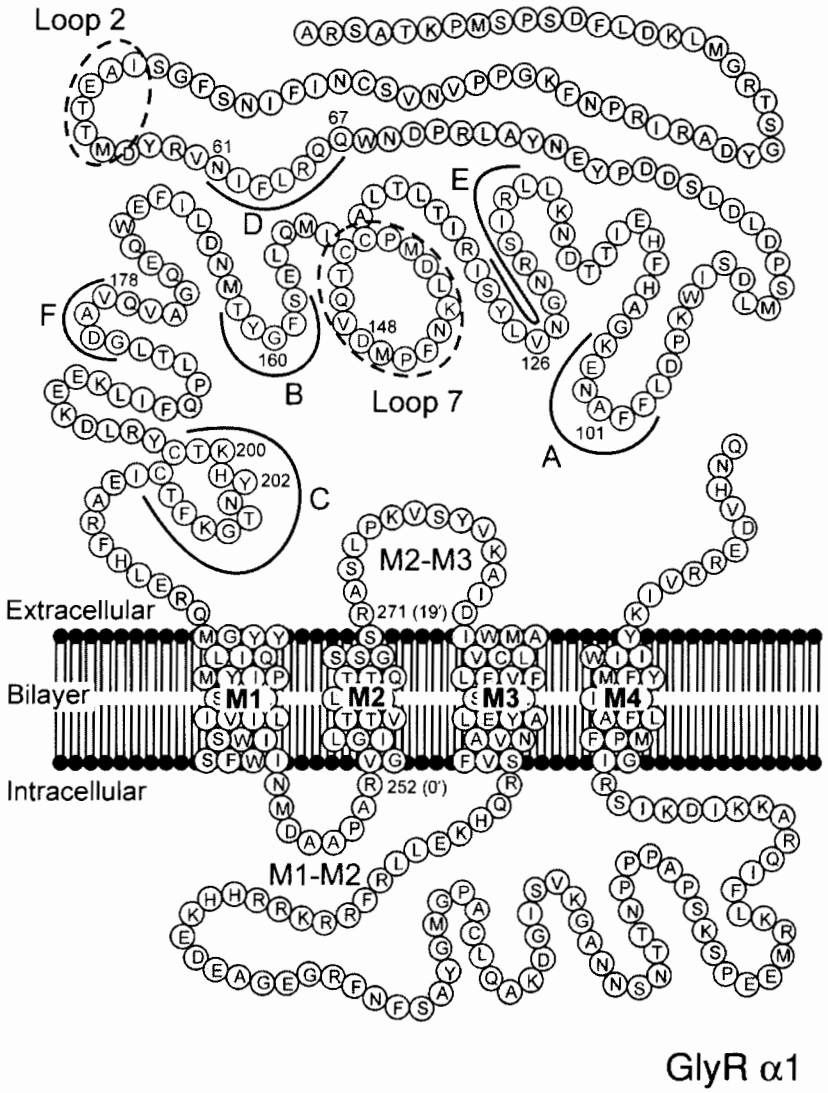

Fig. 9.2 A schematic sequence model of the GlyR, a somewhat typical LGIC, showing the principal ligand-binding domains (A–C) and complementary ligand-binding domains (D–F). These binding domains are indicated with a solid curved line and the residues involved are shown in white. Two of the extracellular loops, considered to be important in signal transduction (loops 2 and 7), are also shown with dashed ellipses, with included resides shown in white. It should be noted that the physical position of some of these extracellular loops, in particular, is likely to be different from that in this illustration, with, for example, loops 2 and 7 probably both close to the transmembrane domain. The transmembrane segments M1–M4 are shown, with the M2–M3 and M1–M2 loops labeled. Redrawn and modified from Fig. 2 of Schofield et al. (1996) to incorporate later data from Brejc et al. (2001) on ligand-binding domains and loops 2 and 7.

Please place this figure-page just after current P.340 (Sec.9.2.1), where it is also referred to elsewhere as being in Sec. 9.2.

until the ligand has dissociated from the receptor and the channel has returned to the closed state.

The four main LGIC types found in vertebrates, and named according to their endogenous agonist, are: the nicotinic acetylcholine receptor (nAChR) channel (so named, because the subgroup of acetylcholine LGICs can selectively be also activated by nicotine), the 5-hydroxytryptamine type 3 receptor (5-HT_3R) channel, the γ-aminobutyric acid receptor channels, types A and C ($GABA_A$R and $GABA_C$R, respectively), and the strychnine-sensitive glycine receptor (GlyR) channel.

To understand how the current passing through an LGIC is generated, consider, for example, either the nAChR or the 5-HT_3R channels, which are predominantly selective to monovalent cations, mainly Na^+ and K^+ ions. For further general details on some of these electrophysiological principles see, for example, Aidley and Stanfield (1996) and Hille (2001). The driving force per mole of ions for ion movement through a membrane is proportional to the electrochemical potential energy difference across that membrane. The electrochemical potential energy ($\bar{\mu}$), which is the free energy per mole of ions, at a particular point in a solution or channel is given by:

$$\bar{\mu} = \mu_o + RT \ln a + zFV, \tag{9.1}$$

where μ_o represents the standard state potential, which will be the same in the two aqueous solutions on either side of the membrane and where a hydrostatic term has been omitted, since it is usually negligible in comparison to the electrical and activity terms. R, T, and F have their usual significance as gas constant, temperature in K, and Faraday constant; z and a represent the valency and activity ($\approx$ concentration in dilute solutions) of the appropriate ion under consideration, and V represents the electrical potential at that point.

In the absence of any large hydrostatic pressure difference across the membrane, the electrochemical potential energy difference across a membrane, between two aqueous solutions, for a mole of ions of species 'j', may readily be shown to be given by:

$$\Delta\bar{\mu}_j = \bar{\mu}_j^i - \bar{\mu}_j^o = zF[V_m - V_j], \tag{9.2}$$

where superscripts 'i' and 'o' refer to the internal and external solutions respectively, V_m is defined by electrophysiologists as the membrane potential, with the convention that it is the potential of the cell interior relative to the outside solution, and V_j is defined as:

$$V_j = (RT/z_jF) \ln\left(a_j^o/a_j^i\right), \tag{9.3}$$

V_j has the dimensions of electrical potential and represents the ~~electrical~~ potential that would just balance the ~~membrane potential, so that there would be no energy difference~~ across the membrane for those ions. Hence, V_j is referred to as the equilibrium

(Nernst) potential for ion j and represents the potential at which those ions would be in equilibrium. The driving force for the movement of ion j across a membrane would be given by $(V_m - V_j)$.

For example, for Na^+, the equilibrium potential, V_{Na}, would be given by:

$$V_{Na} = (RT/F)\ \ln\left(a^{o}_{Na}/a^{i}_{Na}\right), \tag{9.4}$$

since $z_{Na} = 1$. There will be a corresponding equilibrium potential for K^+ in terms of its activities similar to Eq. 9.4 with "Na" replaced by "K". The driving force for Na^+ ion movement is therefore given by $(V_m - V_{Na})$. Nerve and muscle cells, like most other cells under in vivo conditions, have a very large inward driving force on Na^+ ions ($V_m \ll 0$, $V_{Na} \gg 0$; so that $V_m - V_{Na}$ is very much less than 0) and a small outward driving force on K^+ ions (V_m is normally just a little greater than V_K, so that $V_m - V_K$ is only just a little greater than 0) at typical membrane potentials (–70 to –90 mV). Hence, when nAChR or 5-HT_3R channels open, there is a net influx of cations (inward current), due to a large influx of Na^+ ions and only a small efflux of K^+ ions. This net influx of positive ions tends to drive the membrane potential positive (to depolarize the cell) and, if large enough, can exceed the threshold for initiating an electrical impulse, an action potential, in the postsynaptic cell. The nAChR and 5-HT_3R channels are therefore excitatory. In particular, the nAChR channel in muscle cells plays a major role in neuromuscular transmission. In response to a nerve impulse traveling down a motor nerve, there is a release of the neurotransmitter, acetylcholine (ACh) molecules, from the nerve ending. The ACh molecules bind to the nAChRs on the muscle cell membrane, depolarize the muscle cell and normally initiate an action potential in that cell, which, in turn, leads to the muscle contracting. One interesting competitive blocker of the nAChR is the plant alkaloid, curare (D-tubocurarine), used as a paralytic poison in the Amazon and also as a muscle relaxant in surgery (e.g., Hille, 2001). Also, neuronal nAChRs are involved in nicotine addiction (Cordero-Erausquin et al., 2000). The 5-HT_3R is known to be involved in sensory processing, including pain reception and aspects of motor control. Selective 5-HT_3R antagonists are also used in clinical situations as anti-emetic agents to reduce nausea and vomiting (Conley, 1996).

In contrast to the above two excitatory LGICs, the $GABA_AR$, $GABA_CR$, and GlyR channels are predominantly selective to anions, such as Cl^- ions, the major anion in the external solution bathing animal cells. In most, but not all cells, because of the usual very low internal concentration of Cl^- ions, with its concentration gradient more than compensating for the negative membrane potential, there is a net inward driving force $[(V_m - V_{Cl}) > 0]$. Therefore, when $GABA_AR$ and GlyR channels open, there is a net influx of Cl^- ions (outward current), which drives the membrane potential more negative (or provides a conductance shunt), and as a result the effectiveness of any concurrent excitatory signals would be reduced, so that such an excitatory signal may be unable to depolarize the membrane potential sufficiently to initiate an action potential. The $GABA_ARs$, $GABA_CRs$, and GlyRs are therefore normally inhibitory. These inhibitory channels play a major role in the processing

of sensory and motor signals in the central nervous system. Bicucculine and picrotoxin, which block these inhibitory $GABA_AR$ channels, can cause convulsions. In contrast, benzodiazepines (e.g., valium) or barbiturates, which increase the response of $GABA_AR$ to GABA, can have a sedative or calming effect (Mohler et al., 2000). Similarly, GlyR channels are essential, in addition to other functions, for modulating reflex responses important in the maintenance of posture. For example, low doses of the plant alkaloid, strychnine, which can antagonize the GlyR response to glycine, can produce an increased responsiveness to sensory stimuli, whereas high doses can result in exaggerated reflexes, an absence of muscle control, convulsions, and then death (Schofield et al., 1996). There is one particular genetic disease, startle disease, or hyperekplexia, in which the GlyR channel is defective (Schofield et al., 1996). If sufferers of hyperekplexia are suddenly startled, the reduction of this inhibitory modulation can lead to a greatly exaggerated reflex response, which can result in them becoming rigid and falling over.

9.2 Physicochemical Structure

9.2.1 Overall Structure of LGICs

The above LGIC complexes are all pentameric, comprised of five similar subunits, which form a barrel-like structure (Fig. 9.1), with a channel pore running through the middle of the complex. Each subunit is comprised of four transmembrane segments (M1, M2, M3, and M4), as shown in Fig. 9.2, and as indicated in Fig. 9.1B, the channel pore is known to be lined by the M2 segments. There is a large N-terminal hydrophilic extracellular domain, which contains the main ligand-binding region in some subunits. This extracellular domain is connected to the M1 domain. There is a short intracellular loop connecting M1 to M2 and a short extracellular loop connecting M2 to M3 (Fig. 9.2). A long intracellular loop connecting M3 to M4 is thought to be associated with cytoskeletal proteins within the cell (such as rapsyn in the nAChR and gephyrin in the GlyR) that acts as a support structure to control the clustering of the receptors at appropriate regions of the membrane. The five nAChR subunits are α, β, γ, δ, and ε, with some subunits possessing a number of variants ($\alpha 1$–$\alpha 10$, $\beta 1$–$\beta 4$; Alexander et al., 2004). The embryonic muscle nAChR and the *Torpedo* organ nAChR have a stoichiometry of $2\alpha{:}\beta{:}\gamma{:}\delta$ (with two α and one each of β, γ, and δ subunits; Alexander et al., 2004; Miyazawa et al., 2003). In addition, the ligand-binding region is generally located at the interfaces between the α subunit and the γ and δ subunits. Similarly, GlyRs can be heteromeric with a stoichiometry of $2\alpha{:}3\beta$ subunits (Grudzinska et al., 2005), or homomeric with five identical α subunits. Other LGICs known to exist as homomers are some neuronal $\alpha 7$ nAChRs and the $\rho 1$ $GABA_CR$.

The complete amino acid sequences of each of the subunits of these LGICs are known and there is a high degree of sequence identity and similarity between them in the different members of this LGIC family.

In spite of the fact that until recently (see below) there has been no information about the crystal structure of the nAChR, much work has been done to build up a 3-D physical picture of these LGICs using other methods. Nigel Unwin and his colleagues have been extremely successful in such efforts with the nAChRs, using special freezing techniques to drop membrane tubes of densely-packed helically arranged nAChRs from the electric ray *Torpedo* into liquid ethane at below −160°C to "freeze" the nAChRs prior to making electron micrographic measurements (Unwin, 1993). In later experiments, the tubes were sometimes sprayed with a mist of ACh as they were being dropped into the liquid ethane to freeze the channels in the open state prior to the electron microscopy (Unwin, 2003). In both cases, the electron micrographs were scanned with a densitometer, averaged and used to build up optical density arrays of the nAChR channel. The differences between the images in the open and closed state have given some very useful information about the mechanism of channel opening, which will be discussed further in Section 9.4. Computational Fourier techniques were then used to build up a 3-D structure of the nAChR from the different views of the above arrays (Unwin, 2000; Miyazawa et al., 2003). Figure 9.3A shows a reconstructed 2-D image from 0.9 nm resolution electron micrographs, with the suggestion of a kinked α-helical M2 region lining the channel pore within the membrane bilayer. Figure 9.3B and C shows sections of a higher 0.46 nm resolution 3-D image of the bottom cytoplasmic region of the nAChR channel showing the lateral portals or windows between the channel pore and the cell cytoplasm, which have been suggested to at least affect channel conductance in some LGICs.

Recently, a soluble acetylcholine-binding protein (AChBP) from a freshwater snail has been found which shares similar pharmacological properties to the α7 homomeric nAChR. Although lacking the transmembrane (TM) domains, it does share an approximately 20% amino acid sequence identity with the ligand-binding domain of the nAChR and incorporates the LGIC signature Cys-loop (loop 7 in Fig. 9.2). A recent study that replaced the ligand-binding domain of a 5-HT_3R with AChBP revealed that AChBP does indeed replicate the function of a real ligand-binding domain (Bouzat et al., 2004). The crystal structure of AChBP, solved by Sixma and colleagues in 2001 (Brejc et al., 2001), reconciles many years of biochemical and electrophysiological investigations into the LGIC family and is thus considered an accurate template of the LGIC ligand-binding domain. As shown in Fig. 9.4, it consists of five identical subunits arranged symmetrically around a central water-filled vestibule. Each subunit comprises 10 β-sheets arranged in a novel immunoglobulin fold with no significant match to any known protein structure. The dimensions of the AChBP are similar to those previously determined from electron diffraction images of *Torpedo* nAChRs (Miyazawa et al., 1999). Agonist-binding pockets are present at the subunit interfaces, approximately midway between the top and bottom of the protein, and abundant evidence (reviewed in Corringer et al., 2000) identifies these as ligand-binding sites. Three loops (Domains A, B, and C) form the "principal" ligand-binding surface on the one side of the interface and three β-strands (Domains D, E, and F) from the adjacent subunit comprise the "complementary"

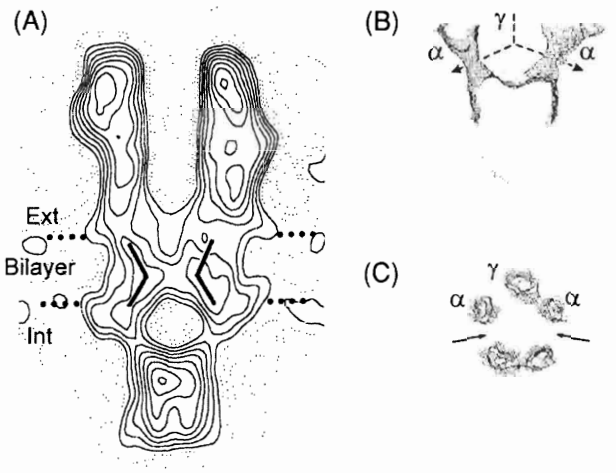

Fig. 9.3 Reconstructed images derived from cryo-electron micrographic images of an nAChR channel. Panel A shows an early reconstruction, at 0.9 nm resolution, of a longitudinal view of the channel, with the black lines shown to depict two kinked-regions of the M2 α-helical parts of two subunits. The position of the membrane bilayer is shown as between the two rows of filled circles and 'Ext' and 'Int' refer to the extracellular and intracellular bilayer interfaces respectively. Panel B, with the higher level of resolution now available, shows part of the very bottom cytoplasmic region of the nAChR channel, at 0.46 nm resolution. This illustrates two of the five lateral portals (tunnels/windows) in the walls of the cavity at the end of the channel pore between the rod-like protrusions at the bottom of the subunits. The rods from the α and γ subunits are shown and the added dashed lines indicate two of the pathways for current flow through the lateral portals. Panel C shows the five rod-like structures in cross-section. The positions of the two largest lateral portals are shown with arrows. Panel A was originally reprinted from Fig. 13a of Unwin (1993) and Panels B and C from part of Fig. 12a and Fig. 12b of Miyazawa et al. (1999) with permission from Elsevier, and the whole figure is now reproduced from Fig. 2 of Barry and Lynch (2005), with copyright permission of [2005] IEEE.

face. Figure 9.4B shows a side-on view of one interface formed between adjacent subunits. The ligand-binding domains are shown for the GlyR in Fig. 9.2.

The structure of the nAChR TM domains was determined by cryo-electron microscopy to a resolution of 0.4 nm by Miyazawa et al. (2003). This structure, depicted later in Fig. 9.11 (in Section 9.4), confirms the long-held view that the TM domains comprise a cluster of four α-helical domains. A water-filled crevice, continuous with the extracellular fluid, is formed between the M1, M2, and M3 domains of each subunit. Abundant evidence identifies this crevice as an alcohol and volatile anesthetic binding site in the $GABA_AR$ and GlyR (Lynch, 2004). The Miyazawa paper did not resolve the structure of the large intracellular loop linking M3 and M4, although it has now been resolved to some degree by Unwin (2005). This domain, which varies considerably in amino acid identity and length among LGIC members, contains phosphorylation sites and other sites responsible for mediating interactions with cytoplasmic factors.

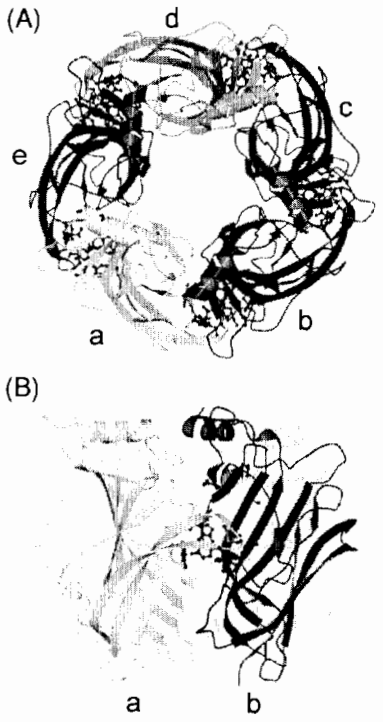

Fig. 9.4 AChBP viewed along the fivefold axis of symmetry toward the membrane. (A) Each subunit is identical ~~and~~ shown in a different color and labeled as a–e. (B) Side view of the same structure with only two subunits (a and b) displayed. The principal ligand-binding domains are on the left side (a) of this interface and the likely ligand-binding residues are shown in ball-and-stick representation. This figure was originally reproduced from Fig. 2 of Brejc et al. (2001), by copyright permission from the Nature Publishing Group, and is now reproduced in monochrome from Fig. 3 of Barry and Lynch (2005), with copyright permission of [2005] IEEE.

, earlier/
i.e., "..identical, earlier .. shown...

9.2.2 Structure of the Channel Pathway

Figure 9.1 shows the pathway for ion movement through a cation-selective channel, like the nAChR, which has opened as a result of the binding of ACh. For an nAChR at a normal resting membrane potential, Na^+ ions will enter the channel vestibule from outside the cell, pass down through a narrow region, which is known as the selectivity filter, before entering a cavity and then passing out into the cytoplasm of the cell via lateral portals (see Fig. 9.3B). K^+ ions will normally move in the opposite direction, because of their oppositely directed driving force.

9.2.3 Other Information from Amino Acid Sequences

In addition to the above structural data, a significant amount of information has been determined from the known amino acid sequences of the subunits of the LGICs.

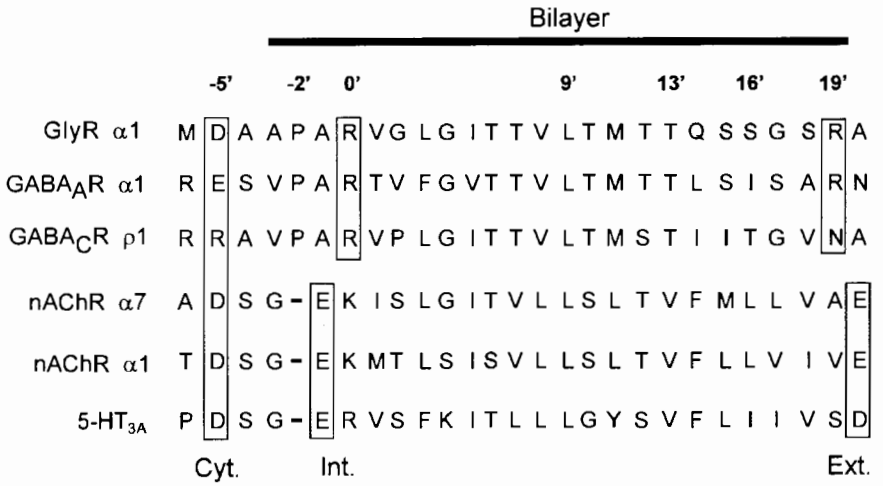

Fig. 9.5 A comparison of the amino acid sequences of the M2 domains of some LGIC subunits, giving their single-letter amino acid codes. The top bar shows the approximate position of the bilayer in relation to this region of the pore. The boxed regions outline many of the critical charged amino acids, the aspartate (D) and glutamate (E) residues being negative and the arginine (R) and the lysine (K) residues being positive. Cyt., Int., and Ext. refer to the cytoplasmic, intracellular and extracellular rings of charge respectively. This is a modified version of Fig. 3 of Keramidas et al. (2004), where details of the references for the sequences of each of the LGICs may be found. The set of numbers with primes represent a convenient standard relative numbering system for the M2 regions of the various subunits, arbitrarily defined with respect to the arginine or lysine residues, in the region of the intracellular charged ring, as being at position 0′. Based on Fig. 3A of Keramidas et al. (2004). This figure has been reproduced from Fig. 4 of Barry and Lynch (2005), with permission of [2005] IEEE.

It was from hydropathy plots of the amino acid sequence of each subunit protein that the presence of the TM domains (M1–M4; see Fig. 9.2) was identified on the basis of the nonaqueous solubility of these regions (e.g., Hille, 2001). Together with our knowledge of the properties of the amino acid residues, data from crystal structure inferred from that of the AChBP (discussed earlier), and structure–function studies to be discussed in detail later, our picture of the physical structure of these LGICs is being considerably extended. For example, if we compare the amino acid sequences of the M2 domains of the different LGICs, as shown in Fig. 9.5, it is clear that the amino acid sequences of the M2 pore regions for each of the main LGIC members are very similar, particularly with respect to the charged regions. Both the cation-selective nAChR and 5-HT$_3$R channels have three rings of negative charge. Each ring of charge arises because there is a negative amino acid residue at the same position in the M2 domains of each of the five subunits (e.g., Fig. 9.5). When the subunits assemble to form a channel, these charged residues from each subunit face in toward the channel pore and form a ring of charged residues in the pore (see Fig. 9.7, later). However, the middle, intracellular, ring also has adjacent positive amino acids, but presumably these are set back somewhat from the surface

of the channel pore and therefore do not contribute significantly to the electrical potential in the pore. In contrast to the above LGICs, the anion-selective GlyR and $GABA_AR$ channels have two rings (intracellular and extracellular) of positive charge, and a negatively charged cytoplasmic ring, which evidence suggests is buried in the protein (Section 9.3.2). In addition, from other amino acid sequence evidence for the nAChR, there are also known to be negative charges lining the cytoplasmic portals (Fig. 9.3), whereas for the GlyR channel there are positive charges in the portal region.

An obvious question is: "What role do all these charged amino acids play in determining ion permeation and selectivity?" This will be discussed in detail in Section 9.3.

9.2.4 Structure–Function Studies

The development of two major technologies has enabled very significant advances to be made in our knowledge of the relationship between the molecular structure of these channels and their functional properties, which in turn has led to a greater understanding of their underlying functional mechanisms.

The first of these technologies has been the patch-clamp technique (Hamill et al., 1981; see the discussion in Jordan, 2006; Chapter 2 in this volume). With such techniques, the current of a single ion channel can be directly measured in pA (10^{-12} A), the single-channel conductance determined in pS (10^{-12} S), and the duration of the average open time of the channel determined in ms. Alternatively, using such techniques, the total current of all the open channels in a very small cell can also now be accurately determined.

The second of these technologies has been molecular biology, and, in particular, site-directed mutagenesis, so that individual (or groups of) amino acids can be deleted, inserted or mutated, with the mutant channels then being expressed in tissue-cultured cells. The effect of such mutations on the electrophysiological properties of these specific channels can then be investigated.

The main part of this chapter will now concentrate on how such techniques have been used to determine how ion permeation and selectivity is controlled in these LGICs (Section 9.3) and how these channels are opened in response to the binding of ligands (Section 9.4).

9.3 Ion Conductances, Permeation and Selectivity

As noted earlier, the cation selective nAChRs and 5-HT_3Rs have three negative rings lining their channel pores, whereas the anion selective $GABA_AR$s, $GABA_CR$s, and GlyRs have two positively charged rings lining their pores. The effect of such charged rings on single-channel conductances, ion permeation, and selectivity will now be discussed.

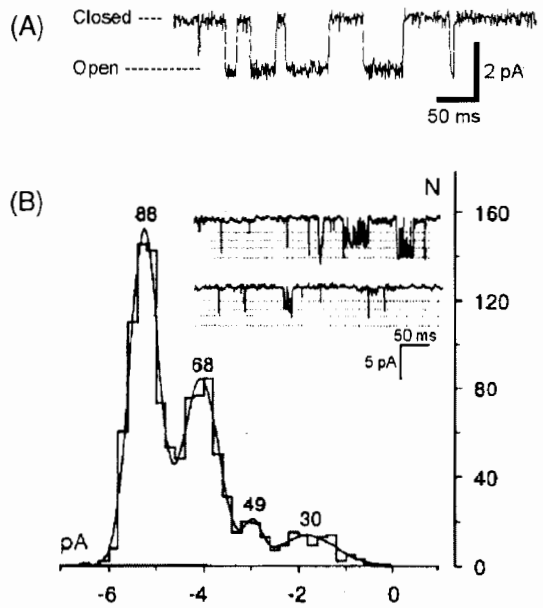

Fig. 9.6 Panel A shows a current record of a toad muscle nAChR channel showing clearly defined transitions between closed and open states (originally modified from a current record of *N*. Quartararo in Fig. 7 of Barry and Gage, 1984) at a potential of −70 mV. Panel B shows current records of normal (wild type; WT) α1 GlyR channels at a potential of −55 mV with a histogram of the current amplitude distribution in pA of the current records (*N* being the frequency for the ordinate), to give the multiple conductance levels in pS at each fitted Gaussian peak (originally a modified version of Fig. 2A of Rajendra et al., 1995). This figure has been reproduced from Fig. 5 of Barry and Lynch (2005), with copyright permission of [2005] IEEE.

9.3.1 Conductances

Patch clamp measurements indicated typical single-channel conductances in the range of about 25–50 pS for neuronal nAChRs (e.g., Conley, 1996) with clear well-defined channel openings with a predominant main conductance level, infrequent sub-conductance levels (e.g., Fig. 9.6A), and typical open times of 5–10 ms or longer. Maximum conductance levels of about 50 pS were observed for heteromeric $\alpha_1\beta$ GlyRs (in human embryonic kidney, HEK, cells) with much shorter (flickery) openings, tending to occur in bursts, and displaying multiple sub-conductance states (Bormann et al., 1993). The main conductance level was dependent on subunit composition and increased to around 90 pS in homomeric α_1 GlyRs (Bormann et al., 1993; cf. Fig. ~~9A~~ and Fig. 2A of Rajendra et al., 1995).

9.6B, /
i.e., "... Fig 9.6B, and ..."

To investigate the role of such charged rings on conductance in the nAChR channel, site-directed mutagenesis was used to change the charge on each ring, by mutating the appropriate residues in the different subunits (e.g., neutralizing a negative charge on the two α subunits, changes the total ring charge by +2 charges, whereas neutralizing it on the single β subunit changes it by +1 charge; Imoto

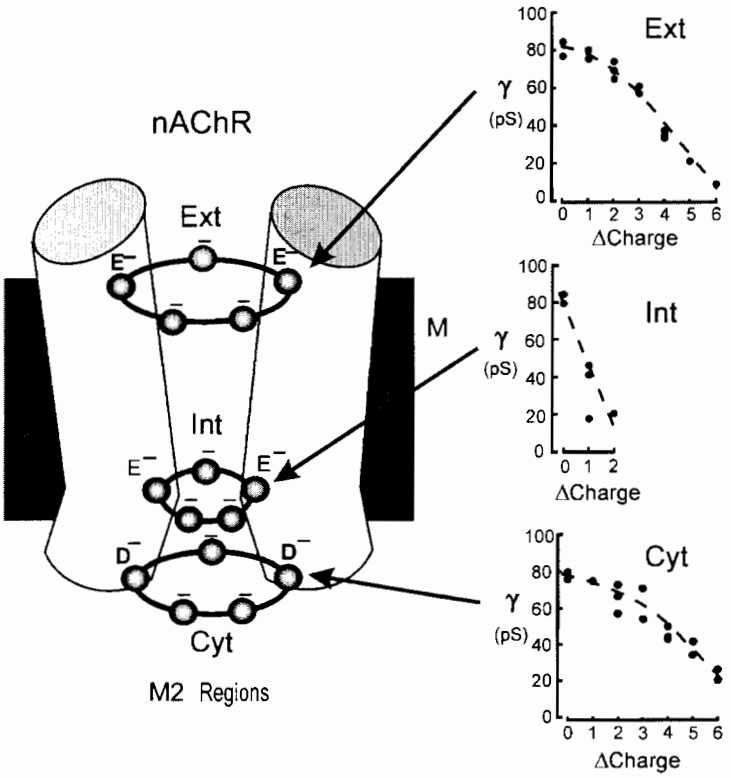

Fig. 9.7 The effect of changing the net charge on each of the three negatively charged rings in the nAChR channel on the single-channel conductance, γ, in pS (10^{-12} S). ΔCharge represents the change in units of electronic charge, the zero value representing the WT nAChR channel. Ext., Int., and Cyt. represent the extracellular, intracellular, and cytoplasmic rings of negative charge, contributed by each charged residue on each of the five subunits (only two of the five M2 helical domains are shown in the schematic diagram), and M indicates the position of the membrane. The three graphs were originally redrawn from Figs. 2d, 2e, and 3b of Imoto et al. (1988) and the figure has been reproduced in monochrome from Fig. 6 of Barry and Lynch (2005), with copyright permission of [2005] IEEE.

et al., 1988). Figure 9.7 shows the graphs of single-channel conductance against the change in charge for various combinations of mutations. The conductance changes are seen to be especially sensitive to changes in net charge at the intermediate ring, where a change of just +2 charges is enough to drop the conductance to 20% of its normal (wild type; WT) value (Fig. 9.7). Similar reductions in single-channel conductance were seen for homomeric α1 GlyR channels, when the five positive charges at the extracellular ring were neutralized (Langosch et al., 1994; Rajendra et al., 1995), though the GlyR channel remained anion-selective. Later experiments (Section 9.3.2) to change the charge on the extracellular ring of a cation-selective GlyR mutant channel showed that the charge on these rings also controlled rectification. A positive extracellular ring of charge produced outward rectification

and a negative one inward rectification (Moorhouse et al., 2002). These charge effects on rectification are discussed further in Keramidas et al. (2004).

It has also been suggested that charges lining the lateral portals at the cytoplasmic end of the channels (Fig. 9.3) may contribute to the channel conductance. In support of this, a series of positive arginines were identified in this region (in the M3–M4 loop) in the 5-HT_3R, which when neutralized or replaced by a negative aspartate, radically increased the inward cation conductance from below 1 pS to about 20 pS (Kelley et al., 2003).

In the $GABA_A$R channel, diazepam and pentobarbitone can also act by increasing single-channel conductance (Eghbali et al., 1997).

9.3.2 Permeation and Selectivity

In the nAChR channel, it has been shown that selectivity between alkali cations could be altered by changing one specific polar residue in the M2 region of the α subunit (Position 2′; see Fig. 9.5) with residues of varying volume (Villarroel et al., 1991). For example, decreasing the volume of the residue to glycine increased the permeability of the channel to the larger Rb^+ relative to the smaller Na^+.

The question still remained: What factors actually determine anion-to-cation selectivity? In an extensive series of mutations, following a comparison of the M2 sequences between the different LGIC members (Fig. 9.5), it has been shown that a minimum of three mutations were able to convert the homomeric α7 nAChR from being cation permeable to being anion permeable (Galzi et al., 1992). The valine at position 13′ was mutated to a polar threonine (V13′T), the glutamate at −1′ was neutralized with an alanine (E-1′A) and a proline was inserted at −2′ (−2′P) (cf. Fig. 9.5). By itself, the glutamate neutralization did remove the calcium permeability (P_{Ca}/P_{Na} decreased from about 10 to <0.02), although the channel was still cation selective. Also by itself, the mutation V13′T actually increased P_{Ca}/P_{Na} and decreased P_{Na}/P_K, and seemed to suggest that an additional desensitized state had become conducting. The precise position of the proline insertion was not absolutely critical, since, for example, if it was inserted at position −4′ instead of at −2′ (along with E-1′A and V13′T), the channel again became anion selective (Corringer et al., 1999). The minimum requirement of the above three mutations, including a proline insertion, suggested a conformational change. The need for such a conformational change seemed to make the precise mechanism for selectivity conversion somewhat unclear (see Galzi et al., 1992; Corringer et al., 1999).

The next LGIC to have its ion charge selectivity inverted was the GlyR (Keramidas et al., 2002). The reverse of the three mutations in the nAChR was introduced at the equivalent locations in the GlyR. The mutations were P-2′Δ, A-1′E, and T13′V (where Δ = deletion). These mutations did convert the GlyR channel from being anion-selective ($P_{Cl}/P_{Na} = 25$) to being cation-selective ($P_{Cl}/P_{Na} = 0.27$). However, the resultant currents were extremely small and brief (requiring noise analysis to determine their single-channel conductance values of 3 pS for inward and 11 pS for outward currents; Keramidas et al., 2000). In addition, the amount

of glycine required as an agonist to ensure a maximum current response was very high (100 mM compared to <0.1 mM for WT GlyRs; Keramidas et al., 2002). The relative permeabilities were determined by doing experiments to dilute the external NaCl concentrations to approximately 50% and 25% of their control values and using the Goldman–Hodgkin–Katz equation to determine the permeability ratios from the voltage required for zero agonist generated current (see discussion in Keramidas et al., 2004). The cation selectivity sequence was $Cs^+ > K^+ > Na^+ > Li^+ \gg Ca^{2+}$, with Ca^{2+} being impermeant (this is a low field strength Eisenman selectivity sequence I or II; see discussion in Jordan, 2006). In such a sequence, the ions with the smaller hydration shell (but larger ionic radius; e.g., Cs^+) are more permeant than the ions with the larger hydration shell (but smaller ionic radius; e.g., Li^+).

Further measurements in the GlyR indicated that the T13′V mutation was actually counterproductive, with the selectivity double mutation (SDM; P-2′Δ and A-1′E) producing a more cation-selective channel ($P_{Cl}/P_{Na} = 0.13$), which had now become permeable to Ca^{2+} ($P_{Ca}/P_{Na} = 0.29$) (Keramidas et al., 2002), and required less glycine to activate it than the selectivity triple mutant (STM) GlyR channel. Although the conductances were similar in magnitude and rectification to the triple mutant GlyR channel, the longer channel openings in the double mutant channel could now be measured directly from current records (Moorhouse et al., 2002). Dissecting the effect of these mutations further, a single proline deletion (P-2′Δ) was found to be unable to invert the ion charge selectivity, though this mutant GlyR channel was less anion selective ($P_{Cl}/P_{Na} = 3.8$) than the WT GlyR ($P_{Cl}/P_{Na} = 25$) (Keramidas et al., 2002). However, a single glutamate mutation (A-1′E) was able to invert the selectivity, giving this cation-selective mutant GlyR a P_{Cl}/P_{Na} value of 0.34 and clarifying a major role for charged residues in determining the ion charge selectivity of these LGICs (Keramidas et al., 2002).

In addition to measurements of anion–cation permeability ratios, measurements were made of the minimum pore diameters of these and other mutant GlyRs. The aim was to investigate whether there were any additional structural changes in the channel, which could be contributing to its ion selectivity. To determine minimum pore diameters, the permeabilities of a range of large organic cations (or anions) were measured for cation-selective (or anion-selective) mutant GlyR channels, in order to determine the maximum dimension of ions, which could just permeate through them (Keramidas et al., 2002; Lee et al., 2003). Such measurements indicated values of ~0.54 nm for the WT GlyR channel (Rundström et al., 1994), ~0.69 nm for the single P-2′Δ GlyR channel (Lee et al., 2003), ~0.65 nm for the A-1′E GlyR channel, and ~0.97 nm for the SDM GlyR channel (Keramidas et al., 2002). Further mutations to change the charge of the external charged ring in the cation-selective SDM GlyR channel gave some interesting results. Neutralizing the external charged ring (P-2′Δ, A-1′E, and R19′A) changed rectification from outward to "linear," whereas making it negatively charged (P-2′Δ, A-1′E, and R19′E), made it inwardly rectifying (Moorhouse et al., 2002). Both of the above results were consistent with the cytoplasmic charged ring being buried in the protein, which is not unreasonable, since this charged ring in the WT GlyR channel is of the inappropriate sign for

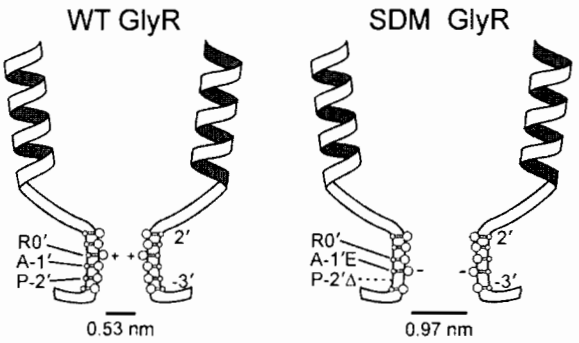

Fig. 9.8 A schematic diagram depicting the selectivity filter region of the GlyR channel at the cytoplasmic (internal) end of two of the M2 segments, where it meets the M1–M2 loop, and the suggested local structural changes which take place when the anion-selective WT GlyR channel is mutated to the cation-selective SDM (A-1′E, P-2′Δ) mutant GlyR channel, with experimentally determined minimum pore diameters shown (see Keramidas et al., 2002; Keramidas et al., 2004). This figure has been reproduced from Fig. 7 of Barry and Lynch (2005), with copyright permission of [2005] IEEE.

an anion-selective channel. The SDM GlyR channel with the negatively charged external ring (P-2′Δ, A-1′E, and R19′E) also had an increased relative calcium permeability compared to the SDM GlyR (Keramidas et al., 2002).

The results in this section indicated that there were two factors determining anion–cation selectivity in these LGICs. The dominant factor was the presence of an effective charged residue in the selectivity filter region, a negative residue making the channel cation-selective and a positive one making it anion-selective. Presumably, the presence of the negative glutamate in the A-1′E mutation caused the adjacent positive arginine (R0′) to move back from the channel surface and so contribute less to the electrical potential in the selectivity filter region of the channel, as indicated in Fig. 9.8. This is supported by the observation in the nAChR channel that the mutations to the K0′ position in the β and γ subunits had no significant effect on cation conductances (Imoto et al., 1988). Ideally, it would have been very instructive to have directly done the mutation R0′E, but mutations of this residue in α1 GlyRs (R0′Q, R0′E, R0′N) failed to express effective channels (Langosch et al., 1994; Rajendra et al., 1995). In addition to the effect of residue charge, the data indicate that the size of the minimum pore diameter of the channel also plays a role, with smaller diameters tending to increase P_{Cl}/P_{Na} and larger ones tending to decrease it (Keramidas et al., 2004). The suggestion was made that in the smaller channel the ions have to be dehydrated to permeate through the filter region (Fig. 9.9). Since it is easier for the larger Cl^- to shed its hydration shell compared to the smaller Na^+ with its much larger hydration shell, this would tend to increase P_{Cl} relative to P_{Na} (Keramidas et al., 2002). In contrast in the larger negatively charged cation-selective channels, Na^+ ions could pass through in a more hydrated state (Keramidas et al., 2002) (Fig. 9.9).

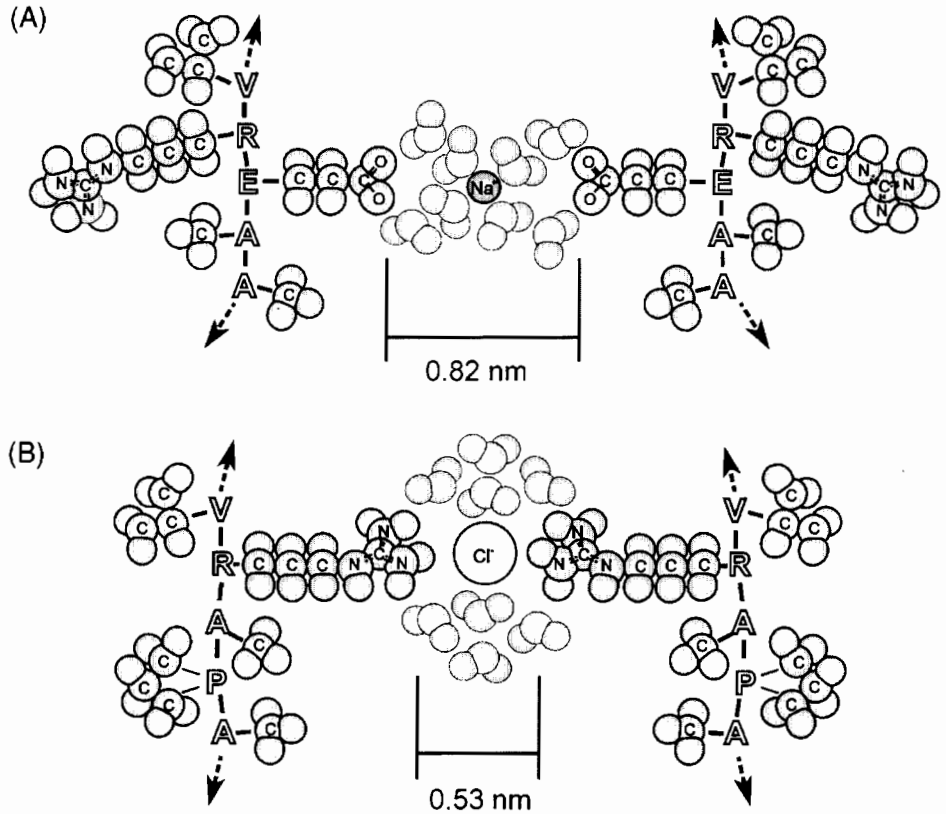

Fig. 9.9 A schematic representation of the selectivity filter region of cation- and anion-selective LGICs between positions 1′ to −3′ and based on data from WT and mutant α1 GlyR channels. Only parts of two M2 domains are shown. Atoms and molecules are drawn approximately to scale and for simplicity only the side chains of the amino acid residues are shown, with the remainder of the residues (the peptide backbone) being represented by the single-letter code for the amino acids. Panel A is intended to depict the situation for the cation-selective (SDM + R19′A) GlyR with the Na^+ ion permeating through the larger diameter filter region without having to be completely dehydrated, whereas for the WT α1 GlyR channel, the Cl^- ion is more readily able to permeate through the smaller diameter filter region in its dehydrated form. This figure has been modified from Fig. 9 of Keramidas et al. (2002) and Fig. 5 of Keramidas et al. (2004).

The relationship between the effect of residue charge and pore diameter is illustrated for WT and mutant GlyRs in Fig. 9.10, where it can be seen that an increase in pore diameter is correlated with a decrease in the relative anion to cation permeability of the channel. However, it may also be seen from this figure that the switch from the channel being predominantly anion-selective to being predominantly cation-selective requires a change in the sign of the effective charge in its selectivity filter region.

Recent measurements have supported similar mechanisms underlying selectivity in the other members of the LGIC family and have added further support to the

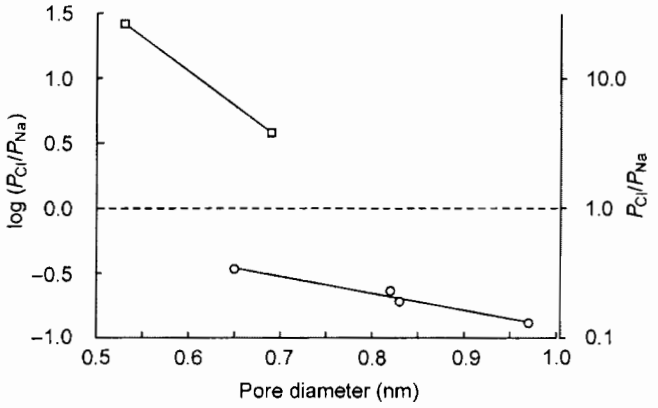

Fig. 9.10 This graph illustrates the relationship between ~~relatively~~ anion–cation permeability and pore diameter, together with the sign of the residue charge in the selectivity filter region, in homomeric α1 GlyRs. The anion-selective GlyR data (open squares) and cation-selective data (open circles) are fitted to two separate lines. The figure shows that increasing pore diameter is correlated with a decrease in the anion–cation permeability ratio, but that a predominantly anion-selective channel requires an effective positive residue charge in the selectivity filter region and a predominantly cation-selective channel an effective negative residue charge. The minimum pore diameter values for the WT GlyR and P-2′Δ GlyR channels were taken from Rundström et al. (1994) and Lee et al. (2003). All other values were taken from Keramidas et al. (2002). The figure has been redrawn from Fig. 4A of Keramidas et al. (2004).

role of the residues in the region from at least −2′ to 2′ as making up the selectivity filter region (see Fig. 9.8). Firstly, a set of triple mutations in the cationic 5-HT_3R, similar to those in the nAChR channel, also made it anion selective (Gunthorpe and Lummis, 2001). In the homomeric ρ1 $GABA_C$R, a single A-1′E mutation made it seemingly nonselective ($P_{Cl}/P_{Na} = 1.3$), whereas a double mutation (P-2′Δ and A-1′E), made it cation-selective ($P_{Cl}/P_{Na} = 0.31$; HEK cell data). Also, in this channel it was possible to directly change the charge at position 0′. Neutralizing this charge made it slightly less anion-selective than the WT ρ1 $GABA_C$R channel, but it still remained anion-selective, whereas replacing the positive charge with a negative one (R0′E), did make the channel weakly cation selective ($P_{Cl}/P_{Na} = 0.4$) (Wotring et al., 2003; see also discussion in Keramidas et al., 2004). ~~Recently, it has also been~~ shown that placing a negative charge in the 2′ position in the ρ1 $GABA_C$R channel (a single mutation of the 2′ proline to a glutamate, P2′E) did invert its charge selectivity from being anion-selective ($P_{Cl}/P_{Na} = 7.1$) to cation-selective (with $P_{Cl}/P_{Na} = 0.08$) (Carland et al., 2004). These results further support the important role of residue charge in controlling the ion selectivity of these LGICs.

9.3.3 Modeling Ion Permeation

To precisely determine the mechanisms underlying ion permeation, it is very instructive to be able to derive a mathematical permeation model to fit to the experimental

data. Permeation models can be classified into three broad classes. These are (1) the classical type of continuum electrodiffusion models, such as the Goldman–Hodgkin–Katz (GHK) equation, the Planck equation, or the Poisson–Nernst–Planck model; (2) kinetic rate theory models, with ions hopping between discrete energy wells, and (3) molecular models such as Brownian dynamics and molecular dynamics, which require knowledge of the precise molecular structure of a channel (see Keramidas et al., 2004, for references).

Clearly, the easiest models to use for determining relative permeability ratios are the electrodiffusion ones, like the GHK equation, and this equation is the one used by most electrophysiologists for this purpose. It is reasonably argued by theoreticians that the underlying Goldman equation, of which the GHK equation is its zero-current form, is dependent on fundamental assumptions, which are likely to be invalid for very narrow channels of sub nm dimensions, such as the LGICs (e.g., 0.6–0.9 nm). However, it has been shown that for membrane potentials, in certain situations and *under zero current conditions*, the permeability ratios, determined by a range of different models, are very similar, in spite of the fact that each model is based on totally different assumptions (Keramidas et al., 2004). These certain situations are the so-called "bi-ionic potentials" where membranes separate two different electrolytes with a common ion (e.g., NaCl:KCl at the same concentration, where P_{Na} and $P_K \gg P_{Cl}$) and so-called "dilution potentials" where the membrane separates the same electrolyte at two different concentrations (e.g., $NaCl_{C1}$:$NaCl_{C2}$, at concentrations C1 and C2). Hence, such derived permeability ratios for these situations seem to be essentially model-independent (Keramidas et al., 2004), and to be similar to parameters which might result from a consideration of the irreversible thermodynamics of anion and cation fluxes through an ion channel.

Nevertheless, it is clearly important to be able to fully understand the mechanisms underlying permeation. To achieve this we need to accurately model ion permeation and current–voltage relationships through such ion channels, taking into account the substantial amount of information that is becoming available about the 3-D molecular structure of the channels. The best practical approach currently is a combination of Brownian dynamics (BD) with other information determined from molecular dynamics (MD). In BD, the total force acting on each ion is calculated from (A) all the electrical forces acting on the ion and from (B) a random fluctuating force due to thermal motion and collisions between ions and water molecules, together with a related frictional viscosity term due to the movement of the ion in the solution. This force acting on the ion is used to calculate the new position and velocity of each ion at a particular time in the channel. This needs to be done in femtosecond (10^{-15} s) time steps for all the ions in the channel and the calculations repeated millions of times, to determine the trajectories of the ions and subsequent ionic fluxes, for different voltages across the channel. O'Mara et al. (2003) were able to run such simulations for WT and some cation-selective mutant α1 GlyR channels and were able to simulate the key permeation features of these channels and particularly the basic role of charged residues in determining ion charge selectivity (O'Mara et al., 2003). Nevertheless, that study was unable to explain the presence

of permeant counterions in these LGIC channels, and their BD models of the above channels only seemed to be able to allow ions of one sign to permeate (i.e., P_{Cl}/P_{Na} was either ∞ for anion-selective WT GlyRs or 0 for cation-selective mutant GlyRs), in spite of the fact that the reversal potentials measured experimentally did not support such conclusions. However, more recently a BD study by Cheng et al. (2005) of both WT and cation-selective mutant GlyRs, based on the same experimental data, but slightly different channel parameters and simulation conditions was able to observe counterion permeation through both sets of channels, with magnitudes consistent both with their reversal potential data and with the experimental anion/cation permeability ratios estimated from reversal potential measurements in those studies (Keramidas et al., 2000, 2002, 2004). It seems most likely that a critical factor in the relationship between relative permeabilities and consistent reversal potentials must lie in the way in which the boundary algorithms, for the ion concentrations on either side of the channel, are implemented.

9.4 Ion Channel Gating

All LGICs contain 2–5 agonist-binding sites. Agonist binding initiates a conformational change that is propagated throughout the protein, culminating in the opening of the channel "gate". The gate is the physical barrier that stops ions from traversing the pore in the unliganded state. This section describes the molecular basis of agonist binding, and the nature of the structural changes that occur once the agonist has bound.

The activation of multi-subunit proteins can be described by two starkly contrasting models: the Monod–Wyman–Changeux (MWC) model (Changeux and Edelstein, 1998, 2005) or the Koshland–Nemethy–Filmer (KNF) model (Koshland et al., 1966). The MWC model proposes that all subunits change conformation simultaneously so the receptor can exist only in either the closed or entirely activated states. Alternatively, the KNF model proposes that each subunit can independently adopt a specific conformation change depending on the number of bound agonist molecules, leading to a series of intermediate states between fully closed and fully open. The KNF model also predicts that different agonists may activate the receptor via different conformational changes. On the other hand, MWC theory predicts a single activated state, although different agonists may stabilize this state to differing degrees. A recent study on the α1 homomeric GlyR found that a full agonist, glycine, and a partial agonist, taurine, both induced similar conformational changes in the external loop linking the M2 and M3 domains (Han et al., 2004). This provides strong evidence in favor of the MWC model.

One of the difficulties in experimentally discriminating between the MWC and KNF models stems from the fact that many oligomeric protein channels are comprised of different subunits. As structurally different subunits would not be expected to respond to agonist binding via identical conformational changes, it can be difficult to experimentally determine whether dissimilar subunits undergo concerted

conformational changes. Taking into account such difficulties, the weight of evidence to date favors an MWC model over a KNF model for the LGIC family (Auerbach, 2003; Changeux and Edelstein, 2005) and most researchers accept that LGIC pore opening is accompanied by the simultaneous activation of all five subunits.

9.4.1 Agonist Binding

Since the ligand-binding domains A–D (see Fig. 9.2 in Section 9.2) of most LGIC members each contain highly conserved aromatic residues, it is likely that all LGIC agonist-binding sites are lined by aromatic rings (Lester et al., 2004). There is abundant evidence that the ACh-nAChR binding reaction is mediated largely by noncovalent "cation-π" electrostatic interactions (Zhong et al., 1998; Celie et al., 2004). In this system, the side chains of the aromatic amino acids (phenylalanine, tyrosine or tryptophan) contribute a negatively charged π surface, while the cation is provided by the agonist. The highly conserved nature of the aromatic groups suggests that this binding mechanism may be broadly applicable across the LGIC family. Indeed, the homologous conserved aromatic residues have been shown to be involved in agonist binding in the $GABA_AR$ (Amin and Weiss, 1993), $GABA_CR$ (Lummis et al., 2005), 5-HT_3R (Spier and Lummis, 2000), and GlyR (Schmieden et al., 1993; Grudzinska et al., 2005). Of course, different LGIC members are highly selective for particular agonists, implying that other receptor-specific binding interactions are also necessary to confer agonist specificity.

The crystal structures of nicotinic agonists (lobeline and epibatidine) and antagonists (α-Conotoxin ImI and methyllycaconitine) complexed with AChBP have recently been published (Hansen et al., 2005). These structures (cf. Fig. 9.2 for the GlyR) confirm that aromatic residues from the principal ligand-binding domains A–C (Fig. 9.2) and complementary ligand-binding domain D form an aromatic "nest" that largely engulfs the ligands. As anticipated from functional studies (Karlin, 2002), the vicinal disulfide between Cys 190 and Cys 191 (in domain C; cf. Fig. 9.2 for the GlyR) and residues in the complementary ligand-binding domains E and F also provide important agonist-binding determinants. The Hansen et al. (2005) study showed that the large antagonists, α-Conotoxin ImI and methyllycaconitine, were also coordinated by the aromatic nest on the principal ligand-binding side, but that there was more variability in the contact sites on the complementary side of the interface (Hansen et al., 2005). A similar study using the peptide antagonist, α-Conotoxin PnIA, revealed a similar picture (Celie et al., 2005). Antagonist binding was not associated with significant movements of domain C, whereas agonist binding resulted in this domain wrapping tightly around the bound agonist (Hansen et al., 2005).

9.4.2 Conformational Changes in the Ligand-Binding Domain

As noted in Section 9.2.1, Unwin obtained low-resolution electron diffraction images of the *Torpedo* nAChR in both the closed and open states (Unwin et al., 1995). Since

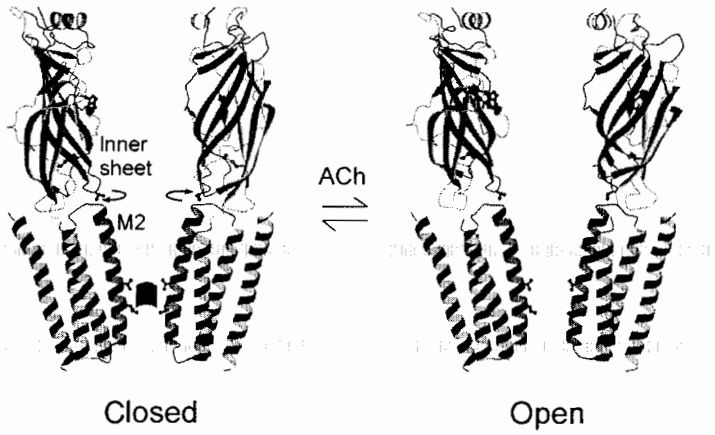

Fig. 9.11 Conformations of the closed (left) and open (right) nAChR, as determined by fitting the polypeptide chains to the electron image density maps of Unwin and colleagues (Unwin et al., 2002; Miyazawa et al., 2003). Moving parts are shown in blue in the original figure. Only two subunits per receptor are shown for clarity. The gate is shown as the curved rectangle (dark pink in the original figure). The TM domain reflects the Miyazawa cryo-EM structure (Miyazawa et al., 2003) and ligand-binding domain is modeled on AChBP (Brejc et al., 2001). This figure was originally reprinted in color by permission of the Federation of the European Biochemical Societies from Fig. 3 of Unwin (2003) and has been reproduced in monochrome from Fig. 8 of Barry and Lynch (2005), with copyright permission of [2005] IEEE.

only the open state structure provided a close match with AChBP, he was able to deduce how the nAChR extracellular domains move upon agonist binding (Unwin et al., 2002). The Unwin model separates the extracellular domain into inner and outer parts. The inner, vestibule-lining part (comprising seven β-sheets) contains most of the inter-subunit contact points plus agonist-binding domain A (see Fig. 9.4, and Fig. 9.2 for the GlyR in Section 9.2). The outer part (which comprises three β-sheets) includes the agonist-binding domains B and C (cf. Fig. 9.2 for the GlyR). Upon agonist binding, the outer part was hypothesized to undergo an upwards tilt around an axis parallel with the membrane plane, while the inner part rotated ~15° in a clockwise direction (when viewed from the synapse) around an axis perpendicular to the membrane plane (Fig. 9.11). The movement of the outer part has the effect of clasping binding domain C around the agonist, virtually burying it in the binding site. A variety of evidence, including direct crystallographic analysis (Celie et al., 2004; Hansen et al., 2005), tryptophan fluorescence (Gao et al., 2005), agonist structure–function relationships (Wagner and Czajkowski, 2001) and molecular structure–function studies (Grutter et al., 2003; Gao et al., 2005), provides strong support for this mechanism. There is, as yet, no independent evidence to support a rotation of the inner sheets, although channel activation has long been considered to be mediated by some kind of relative movement of residues on each side of the subunit interface (Corringer et al., 2000). As noted previously, the recent crystal structures of AChBP complexed with a variety of nicotinic agonists and antagonists reveal

that different surfaces of the complementary binding domain interact with agonists relative to antagonists (Hansen et al., 2005). This implies that agonist binding induces substantial movements in the complementary domain, which is located on the inner sheets. However, no rotation of the inner sheets was observed. Nevertheless, as noted by the authors, it is unclear whether these conformational changes are related to gating since the AChBP lacks the residues that functionally couple ligand-binding with channel activation (Hansen et al., 2005).

The inner sheets (Fig. 9.11) contain two loops that protrude from the bottom of the extracellular part of the structure toward the TM domains (Brejc et al., 2001; Unwin et al., 2002). These loops, numbered 2 and 7, are therefore prime candidates for transmitting agonist-binding information to the activation gate. Loop 7 is also known as the conserved cysteine loop, as mentioned in Section 9.1. Detailed investigations, described below, have begun to unravel the molecular interactions that mediate the information transfer from the agonist-binding site to the activation gate. Studies have focused on the interactions between ligand-binding domain loops 2 and 7, the (extracellular) M2–M3 linker domain, and the (extracellular) pre-M1 domain (see Fig. 9.2 for the GlyR).

9.4.3 Conformational Changes in the Membrane-Spanning Domains

A signal transduction role for the entire M2–M3 domain was first suggested by a systematic site-directed mutagenesis study on the α1 GlyR (Lynch et al., 1997). Although this study showed that mutations to this domain uncoupled the agonist-binding site from the channel activation gate, it provided no information as to whether this domain moved upon channel activation. The substituted cysteine accessibility method (SCAM) was subsequently employed to address the question of domain movement (Karlin and Akabas, 1998). This technique entails introducing cysteine residues one-by-one into the domain of interest. The surface accessibility of cysteines is then probed by highly water-soluble methanethiosulfonate reagents (Karlin and Akabas, 1998). If a functional property of the channel is irreversibly changed by the reagent, then it is assumed that the cysteine lies on the protein surface. Changes in the cysteine modification rate between open and closed states may provide information about the movement of the domain relative to its surroundings. Lynch et al. (2001) employed this approach to show that the surface accessibility of six contiguous residues in the M2–M3 loop of the α1 GlyR subunit experienced an increased surface accessibility in the open state. Surprisingly, a subsequent study by the same group using a similar approach showed that the homologous residues in the GlyR β subunit did not appear to be exposed at the protein–water interface (Shan et al., 2003).

An even more direct measure of protein conformational change is to combine electrophysiology with the quantization of state-dependent changes in the fluorescence of small labels attached to the domain of interest (Gandhi and Isacoff, 2005). Because small fluorophores are often sensitive to the hydrophobicity of their

environment, they may report local structural reorganizations. Such an approach has been employed to monitor changes in the fluorescence of a small fluorophore (rhodamine) tethered to cysteine side chains inserted to the 19′ residue at the N-terminal end of the nAChR M2–M3 domain (Dahan et al., 2004). As expected, this method indeed identified a state-dependent movement in this domain. It also showed that transitions at the 19′ site were not tightly coupled to activation, suggesting that sequential rather than fully concerted transitions occur during channel activation. These results bode well for the use of this technique in characterizing conformational changes in surface domains associated with channel activation. However, it must be acknowledged that we currently know little about the structural reorganization of the M2–M3 domain that occurs during channel activation.

The Auerbach group has pioneered the use of linear free-energy relationships (LFERs) of nAChRs incorporating mutations in various positions (Auerbach, 2003). They have shown that the energy transitions experienced by M2–M3 domain residues are midway between those experienced by residues at the agonist-binding site and the activation gate. The authors conclude that the M2–M3 domain lies at the midpoint of an agonist-initiated conformational "wave" that proceeds from the agonist-binding site to the activation gate (Grosman et al., 2000).

A variety of approaches have been employed to characterize the structural basis of the interactions between the ligand-binding domain and the M2–M3 domain. Research has focused on loops 2 and 7 of the ligand-binding domain as these intercalate directly with the M2–M3 domain. The Miyazawa et al. (2003) nAChR TM structure suggests that a loop 2 hydrophobic side chain fits into the end of the M2 α-helix like a "pin in a socket" Movements of the ligand-binding domain inner sheets would thus rotate the M2 domain to the open state (Figs. 9.11 and 9.12). Functional approaches have also identified strong interactions between the M2–M3 domain and loops 2 and 7 of the ligand-binding domains of GlyRs (see Fig. 9.2) and $GABA_AR$s (Absalom et al., 2003; Kash et al., 2003, 2004). Of particular note, Kash et al. (2003) used mutant cycle analysis to identify an electrostatic interaction between positively charged lysine K279 in the M2–M3 domain and negatively charged D149 in loop 7. The same study also found that cysteines substituted into these positions were able to crosslink in the open state. Together, these results suggest that $GABA_AR$ channel activation is mediated by a decreased distance and hence an increased electrostatic interaction between D149 and K279 (Kash et al., 2003). However, the electrostatic interaction between the corresponding residues in the GlyR is weaker (Absalom et al., 2003), and it is not known whether this mechanism is applicable to other members of the nAChR family. There is also evidence for molecular interactions between loops 2 and 7 and the pre-M1 domain (Kash et al., 2004). However, evidence to date is insufficient to identify any common linkage mechanisms that may pertain to the whole LGIC family.

One way of establishing whether LGIC activation occurs via a universal linkage mechanism between the ligand-binding domain and the M2–M3 loop is to test the functionality of chimeric receptors. It has been shown that the nAChR ligand-binding domain or AChBP attached to the $5\text{-}HT_3R$ TM domains results in

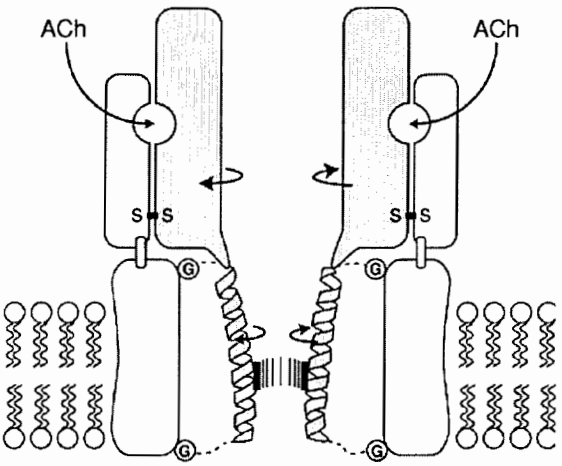

Fig. 9.12 A schematic model for the gating mechanism, depicted in Fig. 9.11. ACh binding induces a rotation in the α subunits, which is transmitted to a hydrophobic barrier or a restriction in the channel through the M2 helices. The helices are linked by flexible loops to the outer protein wall containing glycine residues (G). The two S–S represent disulphide bridge pivots and the moving parts are shown in grey. Originally reprinted from Fig. 6 of Miyazawa et al. (2003) with copyright permission from the Nature Publishing Group, this figure has been reproduced from Fig. 9 of Barry and Lynch (2005), with copyright permission of [2005] IEEE.

functional acetylcholine-gated currents (Bouzat et al., 2004). Similarly, the $GABA_CR$ ligand-binding domain coupled to the GlyR TM domains (Mihic et al., 1997) produces functional channels. However, until functional activation can be demonstrated in chimeras comprising components of both anion- and cation-gated LGICs it is premature to conclude that LGIC activation occurs via a common linkage mechanism.

Low-resolution electron diffraction images of *Torpedo* nAChR originally indicated that the M2 domain incorporated a centrally located kink at the 9′ position (Unwin, 1995) (cf. Fig. 9.3A). The 9′ leucine residue is highly conserved across all LGICs, implying a critical role in channel function. Mutating the 9′ leucines to small polar residues had an equal effect on the ACh sensitivity regardless of which subunit was mutated (Labarca et al., 1995). As binding sites exist at only two of the five subunit interfaces, the implication is that neighboring nAChR subunits interact via their respective 9′ residues. The Miyazawa TM domain structure (Miyazawa et al., 2003) reveals the existence of hydrophobic bonds between the 9′ and 10′ residues of adjacent subunits. These bonds probably maintain the central part of the pore into a fivefold radially symmetrical arrangement that holds the channel closed. It is likely that agonist-induced conformational changes asymmetrically disrupt some of these bonds, leading to a collapse of symmetry and a simultaneous conversion of all M2 domains to the activated state. At this stage it is uncertain how the M2 domains might move during activation. The current prevailing view, shown in Figs. 9.11 and 9.12, is

that the domains rotate about their long axes (Unwin, 1995, 2003; Horenstein et al., 2001; Goren et al., 2004; Taly et al., 2005).

9.4.4 The Gate

As mentioned earlier in this section, the gate is a physical barrier or restriction within the channel, which blocks current flow when the channel is in the closed state. There is currently some uncertainty as to the precise location of this structure. We have also noted that in the open state of LGICs there is a selectivity filter region, which controls the type of ions, which flow through the channel. The question arises: Are the gate and selectivity filter regions physically separate or are they co-localized?

One proposal, originally suggested by Unwin and colleagues (Unwin, 1995; Miyazawa et al., 1999), is that the M2 domains are kinked inwards (see Fig. 9.3A) to form a centrally located hydrophobic gate near the highly conserved 9′ leucine residue. This view is supported by a molecular modeling study (Kim et al., 2004) and by experiments designed to probe the surface accessibility of cysteines introduced into the pore of the 5-HT_3R (Panicker et al., 2002). However, similar experiments on the $GABA_A$R, $GABA_C$R, and nAChR have delimited the gate to the same narrow pore region ($-2'$ to $+2'$) that houses the selectivity filter (Akabas et al., 1994; Xu and Akabas, 1996; Wilson and Karlin, 1998; Filippova et al., 2004).

At present there is no obvious way of reconciling the two sets of observations. One possibility is that the position of the gate may vary among LGIC members.

9.4.5 Modulation of LGIC Receptors

LGIC receptors are modulated by a wide variety of molecules, including endogenous substances of physiological or pathological relevance and exogenous pharmacological probes. In addition to direct protein–protein interactions, LGICs are modulated by post-translational modifications, notably phosphorylation. This involves the covalent attachment of a phosphate group to serine, threonine or tyrosine side chains. A classic means of ion channel modulation is direct channel block: a process whereby a molecule binds to a site in the pore and directly prevents the passage of ions. The molecular basis of quinacrine block of the nAChR has recently been characterized in detail (Yu et al., 2003). Another classic modulatory mechanism is competitive antagonism. This description applies to a molecule that binds to an agonist site but cannot initiate the conformational change required to activate the channel. Strychnine, which binds in the glycine pocket, is a classic competitive antagonist of the glycine receptor (Lynch, 2004). The final category considered here is the "allosteric modulator" This somewhat loose term describes any molecule that alters the conformation of a receptor. By doing so, such modulators can change the function of the receptor in a wide variety of ways. Two examples are the effects of diazepam and pentobarbitone on increasing the single-channel conductance of $GABA_A$, mentioned at the end of Section 9.3.2. Many classical blockers and competitive antagonists also exert allosteric effects.

9.5 Conclusions and Some Questions Still Pending

9.5.1 Ion Conductances, Permeation and Selectivity

It has been shown that changing the net charge on the rings of charge in the LGICs alters their single-channel conductance and that the most sensitive response results from changes at the intracellular ring. For example, decreasing the negative charge in that ring in the cation-selective nAChR radically reduces channel conductivity.

Structure–function selectivity experiments in all of the LGICs have implicated very similar underlying mechanisms with a major role being due to the sign of the charge residues in the ion selectivity filter region (from at least position $-2'$ to $+2'$) close to the intracellular ring. Data for the mutant cation-selective GlyRs also suggest a secondary contribution from changes in the minimum pore diameter in these mutations, with larger diameters tending to increase the cation/anion permeability ratio.

Four pending ion permeation questions follow. (1) What role, if any, do the negative or positive charges lining the cytoplasmic portals play in determining ion selectivity? The experimental evidence outlined in this chapter for the GlyR channel suggests that this may well be a very minor role, but this needs to be fully investigated both for the GlyR channel and other LGICs. (2) Do other ion selectivity mutant LGICs also display equivalent shifts in minimum pore diameter similar to those demonstrated for the GlyR mutant channels? (3) What is the precise physical mechanism for counterion permeation through the selectivity filter region and can this be satisfactorily simulated by Brownian and molecular dynamics studies? (4) Can ion hydration factors be feasibly incorporated into present and future Brownian and molecular dynamics studies in order to explain selectivity between different ions of the same sign in such channels?

9.5.2 Ion Channel Gating

The recently resolved structures of AChBP and the *Torpedo* nAChR TM domains together provide an excellent basis for modeling the structure of LGIC family members. Because these models make precise predictions about the relative spatial positioning of residues, they permit the design of more specific experiments aimed at understanding how LGICs open and close. Hopefully, these new high-resolution models will provide new ways of addressing the following three critical questions. (1) How does the ligand-binding domain move upon agonist binding, and how is this movement transferred to the TM domains? (2) How do the TM domains move as the channel opens and closes? (3) Is the gate located at the same position in all LGIC members?

Acknowledgments

We thank Dr. Trevor M. Lewis for reading this manuscript and acknowledge his very helpful comments and suggestions, and thank both him and Dr. Andrew Moorhouse

for their comments on the previous IEEE manuscript. We also thank the IEEE for permission to use much of the text and the figures of Barry and Lynch (2005).

References

Absalom, N.L., T.M. Lewis, W. Kaplan, K.D. Pierce, and P.R. Schofield. 2003. Role of charged residues in coupling ligand binding and channel activation in the extracellular domain of the glycine receptor. *J. Biol. Chem.* 278:50151–50157.

Akabas, M.H., C. Kaufmann, P. Archdeacon, and A. Karlin. 1994. Identification of acetylcholine receptor channel-lining residues in the entire M2 segment of the alpha subunit. *Neuron* 13:919–927.

Aidley, D.J., and P.R. Stanfield. 1996. Ion Channels: Molecules in Action. Cambridge University Press, Cambridge, UK.

Alexander, S.P., A. Mathie, and J.A. Peters. 2004. Guide to receptors and channels. *Br. J. Pharmacol.* 141:S1–S126.

Amin, J., and D.S. Weiss. 1993. $GABA_A$ receptor needs two homologous domains of the beta-subunit for activation by GABA but not by pentobarbital. *Nature* 366:565–569.

Auerbach, A. 2003. Life at the top: The transition state of AChR gating. *Sci. STKE.* 2003:re11.

Barry, P.H., and P.W. Gage. 1984. Ionic selectivity of channels at the end plate. *Curr. Top. Membr. Transp.* 21:1–51.

Barry, P.H., and J.W. Lynch. 2005. Ligand-gated channels. *IEEE Trans. Nanobiosci.* 4:70–80.

Bormann, J., N. Rundstrom, H. Betz, and D. Langosch. 1993. Residues within transmembrane segment M2 determine chloride conductance of glycine receptor homo- and hetero-oligomers. *EMBO J.* 12:3729–3737.

Bouzat, C., F. Gumilar, G. Spitzmaul, H.L. Wang, D. Rayes, S.B. Hansen, P. Taylor, and S.M. Sine. 2004. Coupling of agonist binding to channel gating in an ACh-binding protein linked to an ion channel. *Nature* 430:896–900.

Brejc, K., W.J. van Dijk, R.V. Klaassen, M. Schuurmans, J. van der Oost, A.B. Smit, and T.K. Sixma. 2001. Crystal structure of an ACh-binding protein reveals the ligand-binding domain of nicotinic receptors. *Nature* 411:269–276.

Carland, J.E., A.J. Moorhouse, P.H. Barry, G.A.R. Johnston, and M. Chebib. 2004. Charged residues at the 2′ position of human GABAC rho 1 receptors invert ion selectivity and influence open state probability. *J. Biol. Chem.* 279:54153–54160.

Celie, P.H., S.E. van Rossum-Fikkert, W.J. van Dijk, K. Brejc, A.B. Smit, and T.K. Sixma. 2004. Nicotine and carbamylcholine binding to nicotinic acetylcholine receptors as studied in AChBP crystal structures. *Neuron* 41:907–914.

Celie, P.H., I.E. Kasheverov, D.Y. Mordvintsev, R.C. Hogg, P. van Nierop, R. van Elk, S.E. van Rossum-Fikkert, M.N. Zhmak, D. Bertrand, V. Tsetlin, T.K. Sixma, and A.B. Smit. 2005. Crystal structure of nicotinic acetylcholine receptor homolog

Barry, P.H. 2006. The reliability of relative anion-cation permeabilities deduced from reversal (dilution) potential measurements in ion channel studies. Cell Biochem. Biophys. 46(2) (October, in press).

2′ ie. prime not apostrophe

AChBP in complex with an alpha-conotoxin PnIA variant. *Nat. Struct. Mol. Biol.* 2:582–588.

Changeux, J.P., and S.J. Edelstein. 1998. Allosteric receptors after 30 years. *Neuron* 21:959–980.

Changeux, J.P., and S.J. Edelstein. 2005. Allosteric mechanisms of signal transduction. *Science* 308:1424–1428.

Cheng, M.H., M. Cascio, and R.D. Coalson. 2005. Theoretical studies of the M2 transmembrane segment of the glycine receptor: Models of the open pore structure and current–voltage characteristics. *Biophys. J.* 89:1669–1680.

Conley, E.C. 1996. The Ion Channels Factbook I—Extracellular Ligand-Gated Channels. Academic Press, London, UK.

Cordero-Erausquin, M., L.M. Marubio, R. Klink, and J.P. Changeux. 2000. Nicotinic receptor function: New perspectives from knockout mice. *Trends Pharmacol. Sci.* 21:211–217.

Corringer, P.J., S. Bertrand, J.-L. Galzi, A. Devillers-Thiery, J.P. Changeux, and D. Bertrand. 1999. Mutational analysis of the charge selectivity filter of the alpha7 nicotinic acetylcholine receptor. *Neuron* 22:831–843.

Corringer, P.J., N. Le Novere, and J.P. Changeux. 2000. Nicotinic receptors at the amino acid level. *Annu. Rev. Pharmacol. Toxicol.* 40:431–458.

Dahan, D.S., M.I. Dibas, E.J. Petersson, V.C. Aeyeung, B. Chanda, F. Bezanilla, D.A. Dougherty, and H.A. Lester. 2004. A fluorophore attached to nicotinic acetylcholine receptor beta M2 detects productive binding of agonist to the alpha delta site. *Proc. Natl. Acad. Sci. USA* 101:10195–10200.

Eghbali, M., J.P. Curmi, B. Birnir, and P.W. Gage. 1997. Hippocampal GABA(A) channel conductance increased by diazepam. *Nature* 388:71–75.

contributes/ Filippova, N., V.E. Wotring, and D.S. Weiss. 2004. Evidence that the TM1-TM2 to the rho1 GABA receptor pore. *J. Biol. Chem.* 279:20906–20914.

Galzi, J.-L., A. Devillers-Thiery, N. Hussy, S. Bertrand, J.P. Changeux, and D. Bertrand. 1992. Mutations in the channel domain of a neuronal nicotinic receptor convert ion selectivity from cationic to anionic. *Nature* 359:500–505.

Gandhi, C.S., and E.Y. Isacoff. 2005. Shedding light on membrane proteins. *Trends Neurosci.* 28:472–479.

Gao, F., N. Bren, T.P. Burghardt, S. Hansen, R.H. Henchman, P. Taylor, J.A. McCammon, and S.M. Sine. 2005. Agonist-mediated conformational changes in acetylcholine-binding protein revealed by simulation and intrinsic tryptophan fluorescence. *J. Biol. Chem.* 280:8443–8451.

Goren, E.N., D.C. Reeves, and M.H. Akabas. 2004. Loose protein packing around the extracellular half of the GABA(A) receptor beta1 subunit M2 channel-lining segment. *J. Biol. Chem.* 279:11198–11205.

Grosman, C., M. Zhou, and A. Auerbach. 2000. Mapping the conformational wave of acetylcholine receptor channel gating. *Nature* 403:773–776.

Grudzinska, J., R. Schemm, S. Haeger, A. Nicke, G. Schmalzing, H. Betz, and B. Laube. 2005. The beta subunit determines the ligand binding properties of synaptic glycine receptors. *Neuron* 45:727–739.

Grutter, T., L. Prado de Carvalho, N. Le Novere, P.J. Corringer, S. Edelstein, and J.P. Changeux. 2003. An H-bond between two residues from different loops of the acetylcholine binding site contributes to the activation mechanism of nicotinic receptors. *EMBO J.* 22:1990–2003.

Gunthorpe, M.J., and S.C. Lummis. 2001. Conversion of the ion selectivity of the 5-HT(3A) receptor from cationic to anionic reveals a conserved feature of the ligand-gated ion channel superfamily. *J. Biol. Chem.* 276:10977–10983.

Hamill, O.P., A. Marty, E. Neher, B. Sakmann, and F.J. Sigworth. 1981. Improved patch-clamp techniques for high-resolution current recording from cells and cell-free membrane patches. *Pflügers Arch.* 391:85–100.

Han, N.L., J.D. Clements, and J.W. Lynch. 2004. Comparison of taurine- and glycine-induced conformational changes in the M2-M3 domain of the glycine receptor. *J. Biol. Chem.* 279:19559–19565.

Hansen, S.B., G. Sulzenbacher, T. Huxford, P. Marchot, P. Taylor, and Y. Bourne. 2005. Structures of *Aplysia* AChBP complexes with nicotinic agonists and antagonists reveal distinctive interfaces and conformations. *EMBO J.* ~~Sep 29~~. ~~[Epub ahead of print]~~ 24:3635–3646

Hille, B. 2001. Ionic Channels of Excitable Cells, 3rd Ed. Sinauer Associates, Sunderland, MA.

Horenstein, J., D.A. Wagner, C. Czajkowski, M.H. Akabas. 2001. Protein mobility and GABA-induced conformational changes in GABA(A) receptor pore-lining M2 segment. *Nat. Neurosci.* 4:477–485.

Imoto, K., C. Busch, B. Sakmann, M. Mishina, T. Konno, J. Nakai, H. Bujo, Y. Mori, K. Fukuda, and S. Numa. 1988. Rings of negatively charged amino acids determine the acetylcholine receptor channel conductance. *Nature* 335:645–648.

Jordan, P.C. 2006. ~~Historical overview~~. *In*: Handbook of Ion Channels: Dynamics, Structure and Applications. S-H. Chung, O.S. Andersen, and V. Krishnamurthy, editors. Springer-Verlag, New York, ~~tbc~~. Ion Channels from fantasy to facts in fifty years

Kandel, E.R., and S.A. Siegelbaum. 2000. Overview of synaptic transmission and signalling at the nerve–muscle synapse: Direct-gated transmission. *In*: Principles of Neural Science, 4th Ed. E.R. Kandel, J.H. Schwartz, and T.M. Jessell, editors. McGraw-Hill, New York, pp. 175–206.

Karlin, A. 2002. Emerging structure of the nicotinic acetylcholine receptors. *Nat. Rev. Neurosci.* 3:102–114.

Karlin, A., and M.H. Akabas. 1998. Substituted-cysteine accessibility method. *Meth. Enzymol.* 293:123–145.

Kash, T.L., M.J. Dizon, J.R. Trudell, and N.L. Harrison. 2004. Charged residues in the beta2 subunit involved in GABAA receptor activation. *J. Biol. Chem.* 279:4887–4893.

Kash, T.L., A. Jenkins, J.C Kelley, J.R. Trudell, and N.L. Harrison. 2003. Coupling of agonist binding to channel gating in the GABA(A) receptor. *Nature* 421:272–275.

Au: Please provide page range for this ref.

pp. 3–29 (Chapter 1, this volume)

Kelley, S.P., J.I. Dunlop, E.F. Kirkness, J.J. Lambert, and J.A. Peters. 2003. A cytoplasmic region determines single-channel conductance in 5-HT_3 receptors. *Nature* 424:321–324.

Keramidas, A., A.J. Moorhouse, C.R. French, P.R. Schofield, and P.H. Barry. 2000. M2 pore mutations convert the glycine receptor channel from being anion- to cation-selective. *Biophys. J.* 79:247–259.

Keramidas, A., A.J. Moorhouse, K.D. Pierce, P.R. Schofield, and P.H. Barry. 2002. Cation-selective mutations in the M2 domain of the inhibitory glycine receptor channel reveal determinants of ion-charge selectivity. *J. Gen. Physiol.* 119:393–410.

Keramidas, A., A.J. Moorhouse, P.R. Schofield, and P.H. Barry. 2004. Ligand-gated ion channels: Mechanisms underlying ion selectivity. *Prog. Biophys. Mol. Biol.* 86:161–204.

Kim, S., A.K. Chamberlain, and J.U. Bowie. 2004. A model of the closed form of the nicotinic acetylcholine receptor m2 channel pore. *Biophys. J.* 87:792–799.

Koshland, D.E., Jr., G. Nemethy, and D. Filmer. 1966. Comparison of experimental binding data and theoretical models in proteins containing subunits. *Biochemistry* 5:365–385.

Labarca, C., M.W. Nowak, H. Zhang, L. Tang, P. Deshpande, and H.A. Lester. 1995. Channel gating governed symmetrically by conserved leucine residues in the M2 domain of nicotinic receptors. *Nature* 376:514–516.

Langosch, D., B. Laube, N. Rundstrom, V. Schmieden, J. Bormann, and H. Betz. 1994. Decreased agonist affinity and chloride conductance of mutant glycine receptors associated with human hereditary hyperekplexia. *EMBO J.* 13:4223–4228.

Lee, D.J.-S., A. Keramidas, A.J. Moorhouse, P.R. Schofield, and P.H. Barry. 2003. The contribution of proline 250 (P-2′) to pore diameter and ion selectivity in the human glycine receptor channel. *Neurosci. Lett.* 351:196–200.

Lester, H.A., M.I. Dibas, D.S. Dahan, J.F. Leite, and D.A. Dougherty. 2004. Cys-loop receptors: New twists and turns. *Trends Neurosci.* 27:329–336.

Lummis, S.C., D. Beene, N.L. Harrison, H.A. Lester, and D.A. Dougherty. 2005. A cation-pi binding interaction with a tyrosine in the binding site of the GABA(C) receptor. *Chem. Biol.* 12:993–997.

Lynch, J.W. 2004. Molecular structure and function of the glycine receptor chloride channel. *Physiol. Rev.* 84:1051–1095.

Lynch, J.W., N.L. Han, J.L. Haddrill, K.D. Pierce, and P.R. Schofield. 2001. The surface accessibility of the glycine receptor M2-M3 loop is increased in the channel open state. *J. Neurosci.* 21:2589–2599.

Lynch, J.W., S. Rajendra, K.D. Pierce, C.A. Handford, P.H. Barry, and P.R. Schofield. 1997. Identification of intracellular and extracellular domains mediating signal transduction in the inhibitory glycine receptor chloride channel. *EMBO J.* 16:110–120.

Caps.
i.e., "... receptor M2 channel..."

Mihic, S.J., Q. Ye, M.J. Wick, V.V. Koltchine, M.D. Krasowski, S.E. Finn, M.P. Mascia, C.F. Valenzuela, K.K. Hansen, E.P. Greenblatt, R.A. Harris, and N.L. Harrison. 1997. Sites of alcohol and volatile anaesthetic action on GABA(A) and glycine receptors. *Nature* 389:385–389.

Miyazawa, A., Y. Fujiyoshi, M. Stowell, and N. Unwin. 1999. Nicotinic acetylcholine receptor at 4.6 A resolution: Transverse tunnels in the channel wall. *J. Mol. Biol.* 288:765–786.

Miyazawa, A., Y. Fujiyoshi, and N. Unwin. 2003. Structure and gating mechanism of the acetylcholine receptor pore. *Nature* 423:949–955.

Mohler, H., D. Benke, J.M. Fritschy, and J. Benson. 2000. The benzodiazepine site of $GABA_A$ receptors. *In*: GABA in the Nervous System: The View at 50 Years. D.L. Martin and R.W. Olsen, eds. Lippincott, Williams and Wilkins, Philadelphia, pp. 97–112.

Moorhouse, A.J., A. Keramidas, A. Zaykin, P.R. Schofield, and P.H. Barry. 2002. Single channel analysis of conductance and rectification in cation-selective, mutant glycine receptor channels. *J. Gen. Physiol.* 119:411–425.

O'Mara, M., P.H. Barry, and S.-H. Chung. 2003. A model of the glycine receptor deduced from Brownian dynamics studies. *Proc. Natl. Acad. Sci. USA* 100:4310–4315.

Panicker, S., H. Cruz, C. Arrabit, and P.A. Slesinger. 2002. Evidence for a centrally located gate in the pore of a serotonin-gated ion channel. *J. Neurosci.* 22:1629–1639.

Rajendra, S., J.W. Lynch, K.D. Pierce, C.R. French, P.H. Barry, and P.R. Schofield. 1995. Mutation of an arginine residue in the human glycine receptor transforms beta-alanine and taurine from agonists into competitive antagonists. *Neuron* 14:169–175.

Rundström, N., V. Schmieden, H. Betz, J. Bormann, and D. Langosch. 1994. Cyanotriphenylborate: Subtype specific blocker of glycine receptor chloride channels. *Proc. Natl. Acad. Sci. USA* 91:8950–8954.

Schmieden, V., J. Kuhse, and H. Betz. 1993. Mutation of glycine receptor subunit creates beta-alanine receptor responsive to GABA. *Science* 262:256–258.

Schofield, P.R., J.W. Lynch, S. Rajendra, K.D. Pierce, C.A. Handford, and P.H. Barry. 1996. Molecular and genetic insights into ligand binding and signal transduction at the inhibitory glycine receptor. *Cold Spring Harb. Symp. Quant. Biol.* 61:333–342.

Shan, Q., S.T. Nevin, J.L. Haddrill, and J.W. Lynch. 2003. Asymmetric contribution of alpha and beta subunits to the activation of alphabeta heteromeric glycine receptors. *J. Neurochem.* 86:498–507.

Spier, A.D., and S.C. Lummis. 2000. The role of tryptophan residues in the 5-hydroxytryptamine(3) receptor ligand binding domain. *J. Biol. Chem.* 275:5620–5625.

Taly, A., M. Delarue, T. Grutter, M. Nilges, N. Le Novere, P.J. Corringer, and J.P. Changeux. 2005. Normal mode analysis suggests a quaternary twist model for the nicotinic receptor gating mechanism. *Biophys. J.* 88:3954–3965.

n/

i.e., "... Changeux..."

Unwin, N. 1993. Nicotinic acetylcholine receptor at 9 A resolution. *J. Mol. Biol.* 229:1101–1124.

Unwin, N. 1995. Acetylcholine receptor channel imaged in the open state. *Nature* 373:37–43.

Unwin, N. 2000. The Croonian Lecture 2000. Nicotinic acetylcholine receptor and the structural basis of fast synaptic transmission. *Philos. Trans. R. Soc. Lond. B. Biol. Sci.* 355:1813–1829.

Unwin, N. 2003. Structure and action of the nicotinic acetylcholine receptor explored by electron microscopy. *FEBS Lett.* 555:91–95.

Unwin, N. 2005. Refined structure of the nicotinic acetylcholine receptor at 4 angstrom resolution. *J. Mol. Biol.* 346:967–989.

Unwin, N., A. Miyazawa, J. Li, and Y. Fujiyoshi. 2002. Activation of the nicotinic acetylcholine receptor involves a switch in conformation of the alpha subunits. *J. Mol. Biol.* 319:1165–1176.

Villarroel, A., S. Herlitze, M. Koenen, and B. Sakmann. 1991. Location of a threonine residue in the alpha-subunit M2 transmembrane segment that determines the ion flow through the acetylcholine receptor channel. *Proc. R. Soc. Lond. B. Biol. Sci.* 243:69–74.

Wagner, D.A., and C. Czajkowski. 2001. Structure and dynamics of the GABA binding pocket: A narrowing cleft that constricts during activation. *J. Neurosci.* 21:67–74.

Wotring, V.E., T.S. Miller, and D.S. Weiss. 2003. Mutations at the GABA receptor selectivity filter: A possible role for effective charges. *J. Physiol.* 548:527–540.

Wilson, G.G., and A. Karlin. 1998. The location of the gate in the acetylcholine receptor channel. *Neuron* 20:1269–1281.

Xu, M., and M.H. Akabas. 1996. Identification of channel-lining residues in the M2 membrane-spanning segment of the GABA(A) receptor alpha1 subunit. *J. Gen. Physiol.* 107:195–205.

Yu, Y., L. Shi, and A. Karlin. 2003. Structural effects of quinacrine binding in the open channel of the acetylcholine receptor. *Proc. Natl. Acad. Sci. USA* 100:3907–3912.

Zhong, W., J.P. Gallivan, Y. Zhang, L. Li, H.A. Lester, and D.A. Dougherty. 1998. From ab initio quantum mechanics to molecular neurobiology: A cation-pi binding site in the nicotinic receptor. *Proc. Natl. Acad. Sci. USA* 95:12088–12093.